

See discussions, stats, and author profiles for this publication at: <https://www.researchgate.net/publication/235895476>

4-Bromo-2-(piperidin-1-yl)thiazol-5-yl-phenyl methanone (12b) inhibits Na⁺/K⁺-ATPase and Ras oncogene activity in cancer cells

ARTICLE in EUROPEAN JOURNAL OF MEDICINAL CHEMISTRY · FEBRUARY 2013

Impact Factor: 3.45 · DOI: 10.1016/j.ejmech.2013.01.046 · Source: PubMed

CITATIONS

4

READS

106

16 AUTHORS, INCLUDING:



Florence Lefranc

Université Libre de Bruxelles

141 PUBLICATIONS 4,128 CITATIONS

SEE PROFILE



Germain Revelant

Université de Haute-Alsace

14 PUBLICATIONS 32 CITATIONS

SEE PROFILE



Céline Bruyère

leucémie espoir recherche

32 PUBLICATIONS 414 CITATIONS

SEE PROFILE



Gilbert Kirsch

University of Lorraine

273 PUBLICATIONS 2,584 CITATIONS

SEE PROFILE



Original article

4-Bromo-2-(piperidin-1-yl)thiazol-5-yl-phenyl methanone (**12b**) inhibits Na^+/K^+ -ATPase and Ras oncogene activity in cancer cells

Florence Lefranc^{a,1}, Zhanjie Xu^{e,1}, Patricia Burth^f, Véronique Mathieu^b, Germain Revelant^e, Mauro Velho de Castro Faria^g, Caroline Noyon^c, Diogo Gomes Garcia^f, Damien Dufour^c, Céline Bruyère^b, Cassiano Felipe Gonçalves-de-Albuquerque^f, Pierre Van Antwerpen^{c,d}, Bernard Rogister^h, Stéphanie Hesse^e, Gilbert Kirsch^{e,*,1}, Robert Kiss^{b,*,1}

^aService de Neurochirurgie, Hôpital Erasme, Université Libre de Bruxelles, Brussels, Belgium

^bLaboratoire de Toxicologie, Université Libre de Bruxelles, Brussels, Belgium

^cLaboratoire de Chimie Pharmaceutique Organique, Université Libre de Bruxelles, Brussels, Belgium

^dPlate-Forme Analytique, Faculté de Pharmacie, Université Libre de Bruxelles, Brussels, Belgium

^eUniversité de Lorraine, Laboratoire d'Ingénierie Moléculaire et Biochimie Pharmacologique, Institut Jean Barriol, FR CNRS 2843, 1 Boulevard Arago, 57070 METZ, France

^fDepartamento de Biologia Celular e Molecular, Instituto de Biologia, Universidade Federal Fluminense, Outeiro de São João Batista, s/n Campus do Valonguinho, Centro-Niteroi, Rio de Janeiro, Brazil

^gDepartamento de Medicina Interna, Faculdade de Ciências Médicas, Universidade do Estado do Rio de Janeiro, Rio de Janeiro, Brazil

^hLaboratoire de Neurobiologie du Développement, GIGA-Neurosciences, Université de Liège, Sart Tilman, B-4000 Liège, Belgium

ARTICLE INFO

Article history:

Received 9 July 2012

Received in revised form

16 January 2013

Accepted 22 January 2013

Available online 16 February 2013

Keywords:

Thiazoles

Thienothiazoles

Perillyl alcohol

In vitro

Na^+/K^+ -ATPase

Ras oncogene

Apoptosis resistance

ABSTRACT

The *in vitro* growth inhibitory activity of 26 thiazoles (including 4-halogeno-2,5-disubstituted-1,3-thiazoles) and 5 thienothiazoles was assessed on a panel of 6 human cancer cell lines, including glioma cell lines. (4-Chloro-2-(piperidin-1-yl)thiazol-5-yl)(phenyl)methanone (**12a**) and (4-bromo-2-(piperidin-1-yl)thiazol-5-yl)(phenyl)methanone (**12b**) displayed ~10 times greater *in vitro* growth inhibitory activity than perillyl alcohol (POH), which therapeutically benefits glioma patients through the inhibition of both α -1 Na^+/K^+ -ATPase (NAK) and Ras oncogene activity. The *in vitro* cytostatic activities (as revealed by quantitative videomicroscopy) displayed by **12a** and **12b** were independent of the intrinsic resistance to pro-apoptotic stimuli associated with cancer cells. Compounds **12a** and **12b** displayed relatively similar inhibitory activities on purified guinea pig brain preparations that mainly express NAK α -2 and α -3 subunits, whereas only compound **12b** was efficacious against purified guinea pig kidney preparations that mainly express the NAK α -1 subunit, which is also expressed in gliomas, melanomas and non-small-cell lung cancers NSCLCs.

© 2013 Elsevier Masson SAS. All rights reserved.

1. Introduction

Gliomas, especially glioblastomas [1], melanomas [2] and NSCLCs [3] are associated with dismal prognoses because they are

intrinsically resistant to pro-apoptotic stimuli [4–6]. Thus, these cancers are also resistant to conventional radiotherapy and chemotherapy [7,8]. In addition, they develop the multidrug resistance (MDR) phenotype during chronic chemotherapy [9–11]. Treatments whose main effects do not relate to the activation of apoptosis are of particular interest to combat these cancers. For example, the alkylating drug temozolomide, which contributes significant therapeutic benefits to glioblastoma patients [12], induces sustained and irreversible pro-autophagic effects in glioma cells [13].

Innovative approaches to combat several types of cancers associated with dismal prognoses involve the inhibition of various types of ion channels, and we pay particular attention to the α -1 subunit of the Na^+/K^+ -ATPase (NAK) in our group [14], which is significantly overexpressed in gliomas [15], melanomas [16], and

Abbreviations: AECs, alveolar epithelial cells; ATCC, American Type Culture Collection; DSMZ, Deutsche Sammlung von Mikroorganismen und Zellkulturen; ECACC, European Collection of Cell Culture; FGF-10, fibroblast growth factor 10; GBM, glioblastoma; GGR, global growth ratio; K^+ -pnppase, K^+ activated-p-nitrophenylphosphatase; MDR, multidrug resistance; MTT, 3-(4,5)-dimethylthiazol-2-yl)-2,5-diphenyltetrazolium bromide; NAK, Na^+/K^+ -ATPase; NSCLC, non-small-cell lung carcinoma; POH, perillyl alcohol; QVM, quantitative videomicroscopy.

* Corresponding author. Tel.: +32 477622083.

** Corresponding author. Tel.: +33 0387315295.

E-mail addresses: kirsch@univ-metz.fr (G. Kirsch), rkiss@ulb.ac.be (R. Kiss).

¹ Authors contributed equally to this article.

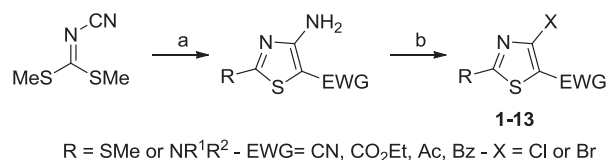
NSCLCs [17]. Impairing NAK alpha-1 subunit activity kills cancer cells, and the effect is more detrimental to cancer cells than to normal cells [15,16]. Such impairment induces irreversible autophagy in glioma cells and lysosomal membrane permeabilization-related cell death in NSCLC cells [14]. In addition, impairing NAK alpha-1 activity represents an efficient approach to killing MDR cancer cells [18].

The most potent NAK ligands include cardiotonic steroids (cardenolides and bufadienolides), which are useful to treat heart failure, but they cannot be used safely as anticancer agents due to their narrow therapeutic indices [14]. In contrast, NAK inhibitors such as perillyl alcohol (POH) [19] are much less potent than cardiotonic steroids, but they nevertheless contribute significant therapeutic benefits to glioma patients [20,21]. In our group, we have adopted a pharmacological strategy that consists of analyzing the *in vitro* growth inhibitory effects of original compounds in a panel of murine and cancer cell lines that include apoptosis-sensitive versus apoptosis-resistant models. Once we have identified compounds that are active against apoptosis-resistant cancer cells, especially glioma apoptosis-resistant ones, we investigate whether these active compounds display anti-NAK activity. Adopting this strategy in the current study, we identified compound **12b**, which decreased the growth of apoptosis-resistant glioma cells, a feature that seems to partly relate to anti-NAK activity. Indeed, the present study describes the design and characterization of the *in vitro* growth inhibitory activity (by means of an MTT colorimetric assay [15–17]) of 31 novel compounds; 26 thiazoles (including 4-halogeno-2,5-disubstituted-1,3-thiazoles) and 5 thienothiazoles were tested against a panel of 6 human cancer cell lines, which included 3 cell lines that display sensitivity to pro-apoptotic stimuli (the MCF-7 breast [22], the PC-3 prostate [22], and the Hs683 oligodendroglioma [23] cancer cell lines) and 3 cell lines that display various levels of resistance to pro-apoptotic stimuli (the U373 glioblastoma [23], the SKMEL-28 melanoma [24] and the A549 NSCLC [25] cell lines). Two compounds (**12a** and **12b**) displayed IC_{50} *in vitro* growth inhibitory concentrations < 100 μ M against all 6 cancer cell lines, and they were further analyzed in terms of anti-NAK activity. The most potent NAK inhibitor, **12b**, was then assayed for anti-Ras oncogene activity because POH, in addition to its anti-NAK activity [19], also inhibits Ras activity [26,27], and Ras represents a promising anticancer target for many cancer types [28], including gliomas [29]. Lastly, computer-assisted phase-contrast microscopy (quantitative videomicroscopy [15,17,23]) was used to determine whether **12b** induced cytotoxic or cytostatic effects on cancer cells.

2. Chemistry

Recently, we described a one-pot, four-step procedure to synthesize 4-amino-2,5-disubstituted-1,3-thiazoles (Scheme 1) [30]. Here, we report the transformation of these compounds to 4-halogeno-2,5-disubstituted-1,3-thiazoles and the synthesis of thieno[2,3-*d*]thiazoles.

The Sandmeyer reaction is one of the most commonly used procedures to convert a primary amine into a halogen. Therefore,



Scheme 1. Synthesis of 4-halogeno-2,5-disubstituted-1,3-thiazoles. Conditions and reagents: (a) (i) Na₂S·9H₂O, DMF, 70 °C, 2 h (ii) X-CH₂-EWG, 70 °C, 2 h (iii) K₂CO₃, 70 °C, 1 h (iv) R¹R²NH; (b) tBuONO, CuX₂, CH₃CN, reflux.

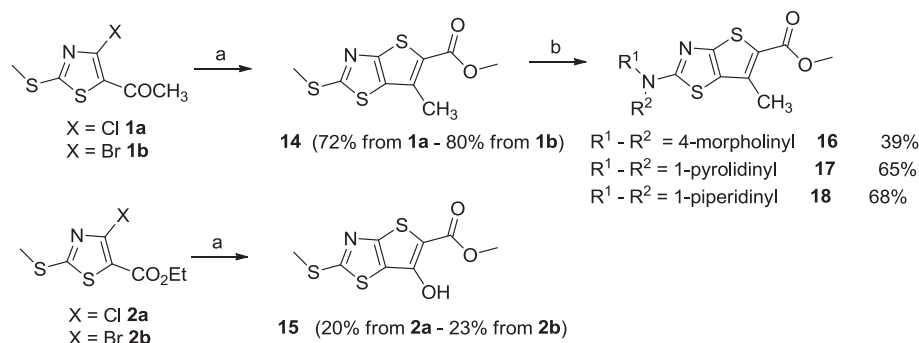
we first tried these classical conditions on several 4-amino-1,3-thiazoles, but the reactions either failed or the yields were rather low. In some cases (e.g., when a cyano group was present at position 5), we obtained some chlorothiazolotriazine derivatives, which resulted from an intramolecular cyclization [31]. We then turned our attention to Doyle's method [32], which we have used successfully to synthesize a thiophene series [33]. This method also works on 2-amino-1,3-thiazoles [34]. 4-Chloro- and 4-bromo-1,3-thiazoles were obtained via this substitutive deamination protocol with moderate to good yields (Scheme 1, Table 1). Generally, bromo derivatives (**1b–13b**) were obtained in higher yields than chloro derivatives (**1a–13a**). This feature could relate to the greater reactivity of CuBr₂ compared to CuCl₂ as emphasized in Ref. [32] (and more precisely in Note 23 of Ref. [32]), in which the authors report that in a competition experiment at 65 °C between CuCl₂ (7.0 mmol) and CuBr₂ (7.0 mmol) that employed *p*-nitroaniline (10 mmol) and *tert*-butyl nitrite (15 mmol), the recovered yield of *p*-bromonitrobenzene (57%) was twice that of *p*-chloronitrobenzene (29%).

The proximity of the halogen and the electron-withdrawing group then allowed several transformations, including access to fused thiazoles. Thieno[2,3-*d*]thiazoles could be synthesized starting either from thiophenes or from thiazoles. For example, 4-bromo-5-nitrothiophene has been used as starting material and converted via thiocyanate to the corresponding thienothiazoles [35]. Thienothiazole-2-carboxamides have been synthesized starting from aminothiophenes [36]. The construction of a thiophene ring onto thiazole has also been described. Often, this ring formation involves a reaction on a chloroformylthiazole; these derivatives have been prepared starting from thiohydantoin [37] or thiazolidine-2,4-dione [38,39]. Here, we reported the condensation of methylthioglycolate on 4-halogenothiazoles (**1a,b** and **2a,b**) and the subsequent cyclization with sodium methylate to afford the corresponding thienothiazoles (**14** and **15**) in moderate to good yields (Scheme 2). We then took advantage of the good leaving group properties of the methylsulfanyl group and performed a S_NAr reaction with secondary amines. Compound **14** was refluxed

Table 1
Synthesis of 4-halogeno-2,5-disubstituted-1,3-thiazoles.

Structure	EWG ^a	X = Cl	Yield (%)	X = Br	Yield (%)
	Ac	1a	80	1b	85
	CO ₂ Et	2a	78	2b	87
	Bz	3a	31	3b	68
	CN	4a	83	4b	81
	Ac	5a	42	5b	55
	CO ₂ Et	6a	43	6b	40
	Bz	7a	61	7b	76
	CN	8a	52	8b	76
	CO ₂ Et	9a	54	9b	64
	Bz	10a	66	10b	71
	CN	11a	48	11b	91
	Bz	12a	59	12b	93
	CN	13a	50	13b	76

^a EWG = electron withdrawing group.



Scheme 2. Synthesis of thieno[2,3-d]thiazoles. Conditions and reagents: (a) $\text{HSCH}_2\text{CO}_2\text{Me}$, MeONa ; (b) $\text{R}^1\text{R}^2\text{NH}$, reflux.

with excess amine overnight and led to compounds **16–18** in 39%–68% yields (Scheme 2).

3. Results

3.1. Determination of the *in vitro* growth inhibitory IC_{50} concentration

Of the 31 compounds synthesized for this study, 16 displayed an IC_{50} *in vitro* growth inhibitory concentration $< 100 \mu\text{M}$ in at least one of the 6 cancer cell lines analyzed (Table 2). The remaining 15 compounds displayed IC_{50} concentrations $> 100 \mu\text{M}$ in each of the 6 cell lines analyzed (data not shown).

POH displayed IC_{50} inhibitory concentrations $> 1000 \mu\text{M}$ in each of the 6 cell lines analyzed (Table 2). In fact, of the 31 compounds synthesized, only **12a** and **12b** displayed IC_{50} concentrations $< 100 \mu\text{M}$ for each of the 6 cell lines analyzed (Table 2). In addition, **12a** and **12b** displayed similar *in vitro* growth inhibition toward not only those cancer cell lines with various levels of resistance to pro-apoptotic stimuli (i.e., U373 glioblastoma [23], SKMEL-28 melanoma [24] and A549 NSCLC [25] cells) but also those lines that are sensitive to pro-apoptotic stimuli (i.e., MCF-7 breast [22] and PC-3 prostate [22] cancer, and Hs683 oligodendroglioma [23] cells; Table 2).

3.2. Evaluation of the *in vitro* growth inhibitory IC_{50} concentration of **12a** and **12b** in normal astrocytes

Primocultures of mouse normal astrocytes were established as validated previously [40] and detailed in the Materials and Methods. Compounds **12a** and **12b** were thus assayed by means of the MTT colorimetric assay on normal mouse astrocytes at 0 (control), 30, 60 and $300 \mu\text{M}$ without reaching growth inhibition below 50% (data not shown). At $300 \mu\text{M}$, the *in vitro* growth inhibition induced by **12a** and **12b** were 86 ± 4 and $68 \pm 6 \mu\text{M}$, respectively. Compound **12a** and **12b** thus displayed bioselectivity indices > 5 in terms of *in vitro* growth inhibition between normal and tumor astrocytes.

3.3. *In vitro* stability determination for compounds **12a** and **12b**

The stability of compounds **12a** and **12b** was determined as detailed in the Materials and Methods. Fig. 1 shows that compound **12a** remained stable over time (72 h) in both water and RPMI cell culture media, while compound **12b** degraded over time. A comparison of the data in Table 1 with those in Fig. 1 suggests that the degradation process observed for compound **12b** compared to compound **12a** did not impair its *in vitro* growth inhibitory activity in various cancer cell lines.

3.4. Evaluation of the cytotoxic versus cytostatic nature of the compounds in this study

As indicated above, only 2 compounds, **12a** and **12b**, displayed IC_{50} growth inhibitory concentrations $< 100 \mu\text{M}$ for each of the 6 cancer cell lines analyzed (Table 2). These 2 compounds were thus analyzed by quantitative videomicroscopy, which revealed that their effect is cytostatic rather than cytotoxic in Hs683 glioma cells, as illustrated by the morphological analyzes in Fig. 2. Indeed, Fig. 3 indicates that **12a** (Fig. 3A) and **12b** (Fig. 3B) delayed Hs683 population growth: calculations of the global growth ratio (GGR; see the legend to Fig. 3) revealed that at $40 \mu\text{M}$ **12a** (Fig. 3C) and **12b** (Fig. 3D) decreased the growth of Hs683 cell populations by $\sim 40\%$. This growth inhibition began on the 48th hour of cell culture and remained until the 72nd hour of culture (Fig. 3C, D). Compounds **12a** and **12b** both exhibited GGR indices of 0.6 (see the legend to Fig. 3) at $40 \mu\text{M}$; this value was in agreement with the IC_{50} concentrations ($\sim 40 \mu\text{M}$) obtained from the MTT colorimetric assay on Hs683 glioma cells (Table 2).

3.5. Inhibition of the Na^+/K^+ -ATPase activity

Compounds **12a** and **12b** displayed inhibitory effects on the growth of various cancer cell lines when compared to POH (Table 2). NAK inhibitory activity was analyzed at a concentration of 1 mM, i.e., the concentration used to demonstrate POH-related anti-NAK activity [24]. Compounds **12a** and **12b** displayed inhibitory activity $> 50\%$ at 1 mM on purified guinea pig brain NAK (Fig. 4A), whereas only compound **12b** displayed inhibitory activity $> 50\%$ at 1 mM on purified guinea pig kidney NAK (Fig. 4B). As a benchmark, Fig. 4A, B also include the inhibition obtained with 1 mM POH.

As shown in Fig. 4C, compound **12b** inhibited purified kidney and brain NAK with some differences. The NAK IC_{50} concentration for **12b** was approximately 0.25 mM for the purified brain enzyme (including mainly α_2 and α_3 NAK isoforms) and approximately 0.35 mM for the whole brain homogenate (Fig. 4C). However, **12b** displayed a lower inhibitory potency for the kidney α_1 isoform. In this case, the **12b**-related anti-NAK IC_{50} concentration was approximately 0.55 mM for both the purified and the homogenate kidney enzymes (Fig. 4D). Fig. 4C and D also show that the ouabain-insensitive Mg^{++} ATPases in the brain and kidney tissue homogenates were not affected within the range of drug concentrations tested.

Kinetic studies were performed to evaluate the influence of a fixed concentration of compound **12b** on the activation of brain- or kidney-purified NAK by Na^+ , K^+ and ATP (Fig. 5); the results revealed that **12b** interacts by non-competitive inhibition with both ions. Double reciprocal plots also demonstrated that

Table 2
Characterization of the *in vitro* growth inhibitory activity of 4-halogeno-2,5-disubstituted-1,3-thiazoles and thieno[2,3-*d*]thiazoles on a panel of six human cancer cell lines.

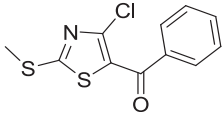
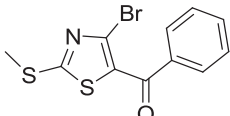
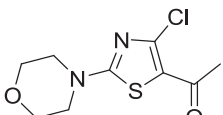
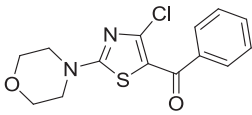
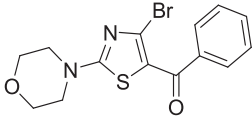
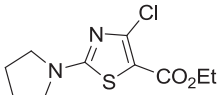
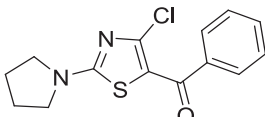
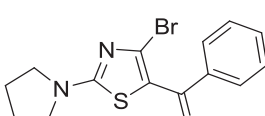
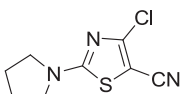
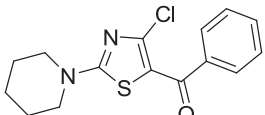
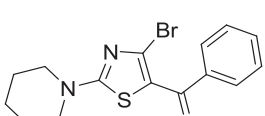
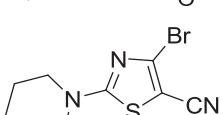
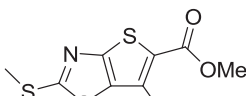
Compound ^a	Chemical structure	Growth inhibitory IC ₅₀ (μM) concentration after culturing the cancer cells for 72 h with the compound of interest ^b						
		MCF-7	A549	PC-3	U373	Hs683	SKMEL-28	Mean ± SEM
3a		91	*	*	*	*	*	>99
3b		67	97	*	89	*	*	>92
5a		88	*	*	83	*	*	>95
7a		70	78	*	92	*	*	>90
7b		51	84	*	*	93	*	>88
9a		79	61	78	*	54	82	>76
10a		63	50	*	82	44	98	>73
10b		69	97	*	*	*	*	>94
11a		99	*	*	*	*	*	>99
12a		56	41	69	96	36	91	65 ± 10
12b		35	48	62	78	38	91	59 ± 9
13b		77	93	*	*	84	*	>92
14		69	78	90	92	79	*	**

Table 2 (continued)

Compound ^a	Chemical structure	Growth inhibitory IC ₅₀ (μM) concentration after culturing the cancer cells for 72 h with the compound of interest ^b						Mean ± SEM
		MCF-7	A549	PC-3	U373	Hs683	SKMEL-28	
16		78	96	*	*	92	*	**
17		56	86	*	89	91	*	**
18		90	*	93	*	*	*	**
POH		**	**	**	**	**	**	>1000

* > 100 μM; ** > 1000 μM.

^a Only those compounds with an IC₅₀ concentration < 100 μM on at least one of the six cancer cell lines are reported in Table 2. Thus, those compounds that displayed IC₅₀ concentrations > 100 μM on each of the six cell lines analyzed are not reported in Table 2. The IC₅₀ concentrations of perillyl alcohol (POH), a reference compound in the current study, are reported in Table 2.

^b The *in vitro* growth inhibitory IC₅₀ concentrations were determined using the MTT colorimetric assay. The human cell lines include the MCF-7 breast cancer (DSMZ code ACC115), the A549 NSCLC (DSMZ code ACC107), the PC-3 prostate cancer (DSMZ code ACC465), the U373 glioblastoma (ECACC code 08061901), the Hs683 oligodendroglioma (ATCC code HTB-138) and the SKMEL-28 melanoma (ATCC code HTB-72) cell lines.

compound **12b** acted on purified NAK through an uncompetitive inhibition toward the substrate ATP, regardless of the enzyme origin.

K⁺-activated-p-nitrophenylphosphatase (K⁺-pnppase) activity, which measures phase II of the catalytic NAK cycle, was not inhibited by **12b** in the kidney purified preparations, whereas the brain enzyme was affected (Fig. 6).

3.6. Compound **12b** inhibits Ras oncogene activity

Compound **12b** displays *in vitro* growth inhibitory activity with an IC₅₀ < 100 μM on each of the 6 cancer cell lines tested, an effect that was independent of the cell lines' resistance to pro-apoptotic stimuli (Table 2). In addition, **12b** also displayed inhibitory

activity on the α1 NAK subunit (Fig. 4B). As detailed in the Discussion, NAK and Ras interplay to cross-regulate each other's activity. We therefore analyzed the anti-Ras activity of **12b** and used POH as a dual reference compound for anti-Ras activity [26,27] and anti-α1 NAK subunit activity [19]. The data in Fig. 7 show that at 40 μM (the MTT colorimetric assay IC₅₀ concentration; Table 2) **12b** reduced the Ras activity of Hs683 glioma cells by > 50%; this effect was more rapid and efficient than the anti-Ras activity of 2 mM POH.

4. Discussion

Targeting the ion channels overexpressed in chemoresistant cancers is a new anti-cancer strategy [50]. One promising target is the α1 NAK channel subunit [14], which is overexpressed in gliomas [15], melanomas [16], NSCLCs [17] and other cancer types [14]. The most potent α NAK subunit inhibitors are related to cardiotonic steroids, which are useful for treating heart failure but have narrow therapeutic indices [14]. Therefore, these compounds cannot be used safely as anticancer agents, even if the potential of these compounds as anticancer drugs [41–43], including drugs for MDR cancers [18], are heavily emphasized. Non-cardiotonic, steroid-related compounds also inhibit NAK activity, although the effect is less pronounced than for cardiotonic steroids [14]. Non-cardiotonic, steroid-related drugs include coumestans, iantherans, gossypol, aplysiallene, kaur-16-en-19-oic acid derivatives and dienome A. Among these drugs, *in vitro* anticancer activity has already been demonstrated for gossypol, kaur-16-en-19-oic acid derivatives and dienome A (see Ref. [14] for review). More recently, anti-NAK activity has been reported for POH [19], a monoterpene found in the essential oils of lavender, peppermint, spearmint, sage, cherries, cranberries, lemongrass, and wild bergamot [44]. POH also displays

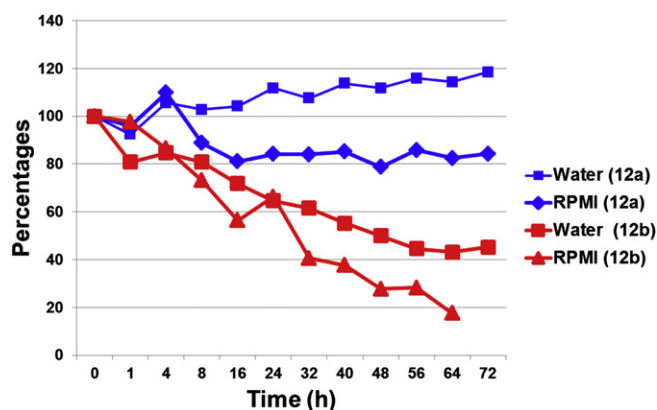


Fig. 1. Stability analyzes of compounds **12a** and **12b** over 72 h in water versus RPMI cell culture medium.

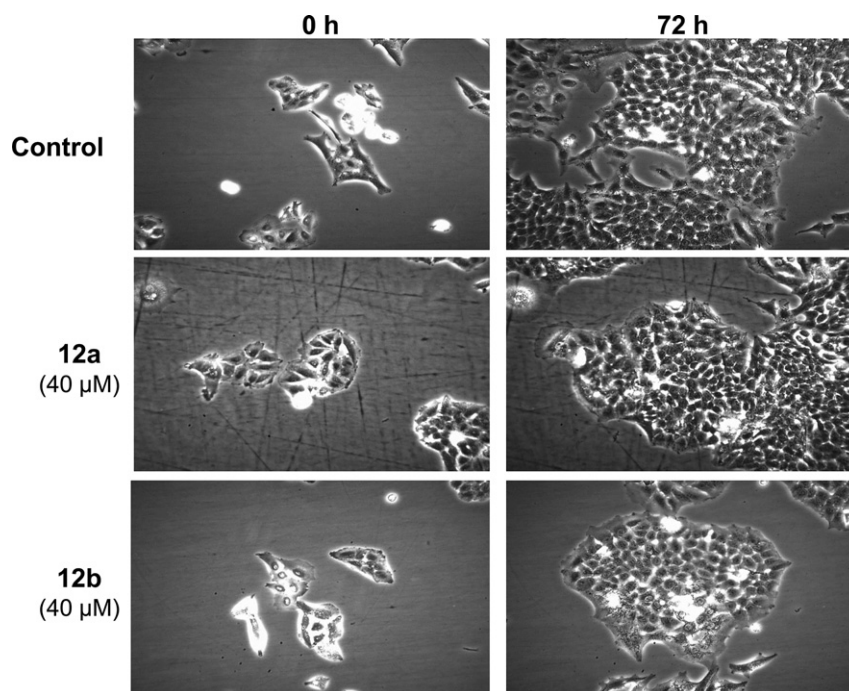


Fig. 2. Morphological illustrations (200× magnification) of the growth patterns of human Hs683 glioma cells cultured for 72 h in the absence (control) or the presence of either 40 μM **12a** or 40 μM **12b**. The morphological images were recorded by computer-assisted phase-contrast microscopy (quantitative videomicroscopy).

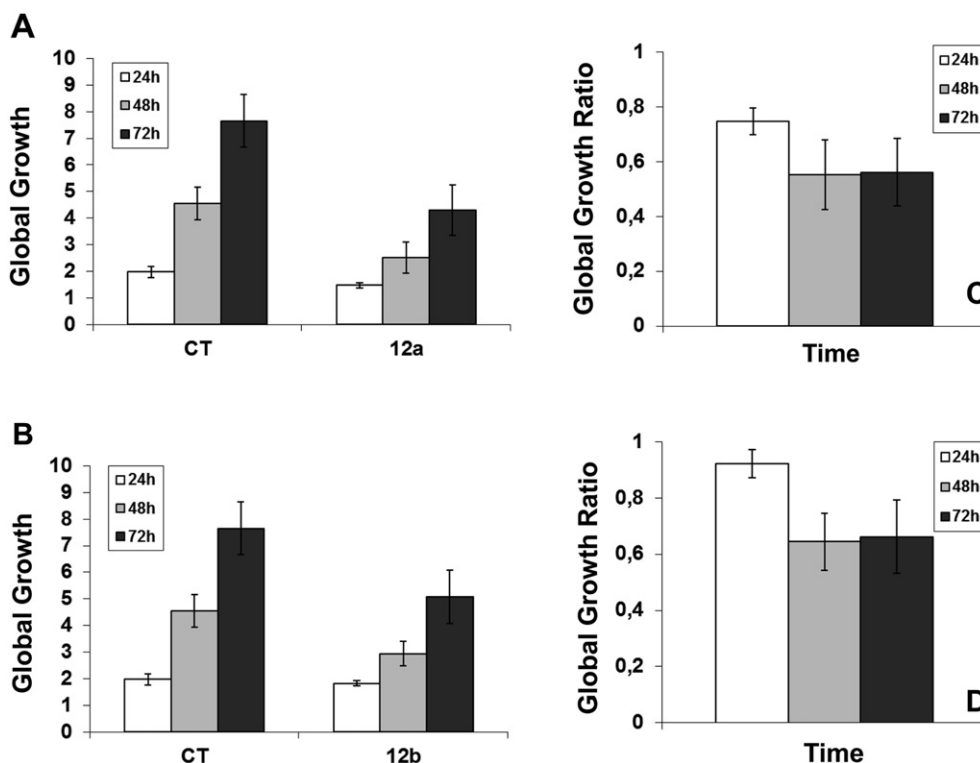


Fig. 3. Based on the quantitative videomicroscopy-related morphological images (see Fig. 2), we calculated the global growth rates of Hs683 glioma cells left untreated (control) or treated with either 40 μM **12a** (A) or 40 μM **12b** (B) for 72 h. One image was digitized every 4 min, so a total of 1080 digitized images were recorded for each experimental condition; each condition was performed in triplicate. All videomicroscopy experiments were performed in parallel; thus the controls in Fig. 3A and B are identical. The global growth rates therefore correspond to the ratio of the mean number of cells present in the 1080th image to the number of cells present in the first image (at 0 h). We divided the ratios obtained from the **12a**- (C) or **12b**- (D) treated experiments by the ratio obtained in the control, enabling the global growth ratio (GGR) index to be calculated. The GGR value of 0.6 in Figs C and D means that 60% of Hs683 glioma cells grew in the treated experiment compared to the control over a 72-hr observation period.

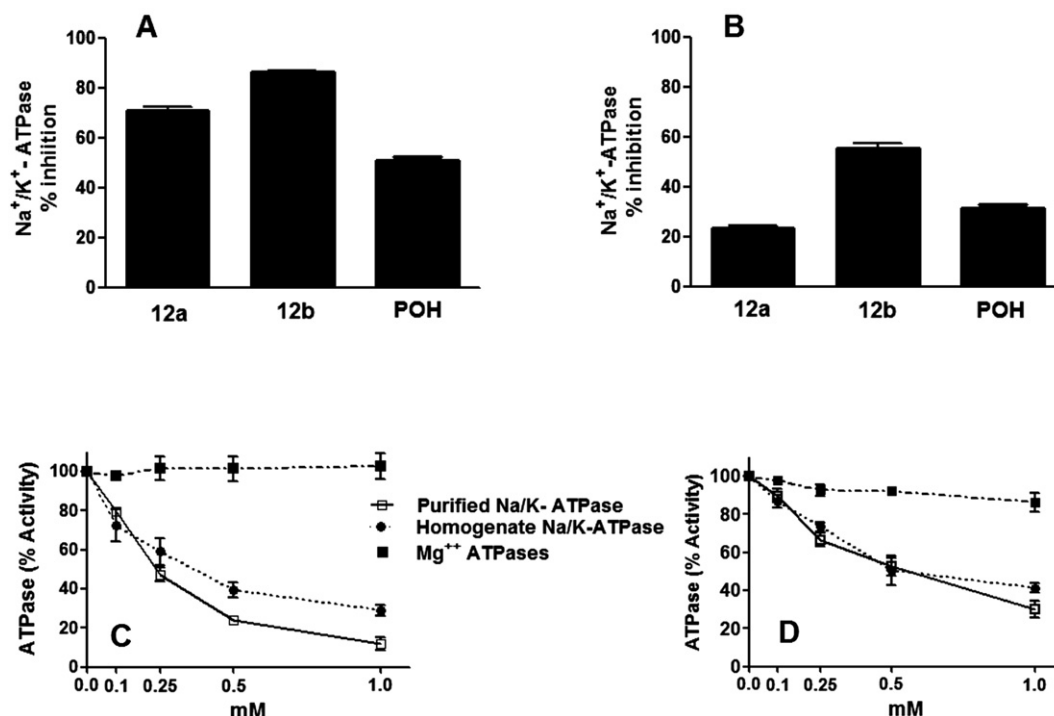


Fig. 4. The inhibition of purified brain (A) and kidney (B) Na⁺/K⁺-ATPase by 1 mM of compounds **12a**, **12b** and POH. Each bar indicates the mean \pm SEM of 5 different experiments. (C) Purified brain Na⁺/K⁺-ATPase, brain homogenate Na⁺/K⁺-ATPase and brain homogenate Mg⁺⁺ ATPase inhibition by **12b**. (D) Purified kidney Na⁺/K⁺-ATPase, kidney homogenate Na⁺/K⁺-ATPase and kidney homogenate Mg⁺⁺ ATPase inhibition by **12b**. Each point in C and D is the mean \pm SEM of 3 different experiments.

anti-Ras activity [26,27], and, as explained below, NAK and Ras activity are closely connected.

In the present study, we have focused on distinct types of thiazoles. Among those tested, (4-chloro-2-(piperidin-1-yl)thiazol-5-yl)(phenyl)methanone (**12a**) and (4-bromo-2-(piperidin-1-yl)thiazol-5-yl)(phenyl)methanone (**12b**) displayed higher than a 10-fold increase in growth inhibition *in vitro* on a panel of 6 human cancer cell lines than POH (Table 2). In addition, the *in vitro* growth inhibitory activity displayed by **12a** and **12b** was independent of the cancer cell lines' resistance (or sensitivity) to pro-apoptotic stimuli

(Table 2). Compounds **12a** and **12b** displayed relatively similar inhibitory activities on purified guinea pig brain preparations (Fig. 4), which overexpressed the $\alpha 2$ and $\alpha 3$ NAK subunits [19]. In contrast, only compound **12b** was efficacious against purified guinea pig kidney preparations, which, like glioma cells [15], melanoma cells [16] and NSCLC cells [17], contain only the $\alpha 1$ NAK subunit [19].

Compound **12b** also displayed anti-Ras activity that was approximately 40 times more pronounced than the anti-Ras activity of POH (Fig. 7).

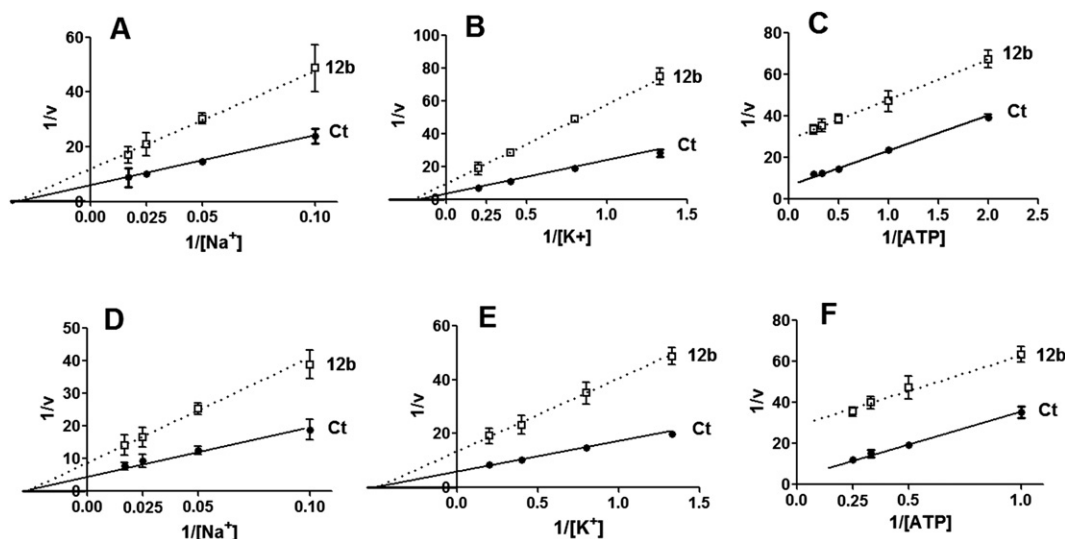


Fig. 5. The influence of compound **12b** on the activation of purified brain Na⁺/K⁺-ATPase by Na⁺ (A), K⁺ (B) and ATP (C). The influence of **12b** on the activation of purified kidney Na⁺/K⁺-ATPase by Na⁺ (D), K⁺ (E) and ATP (F). Each point is the mean \pm SEM of 3–6 different experiments.

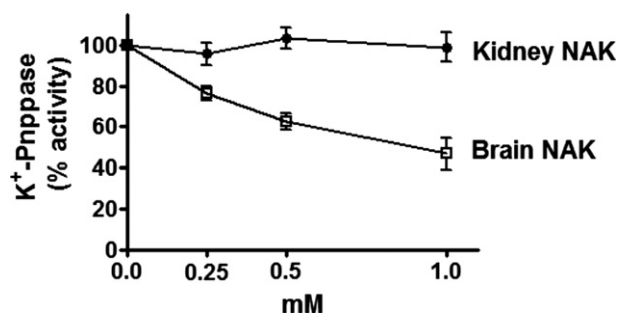


Fig. 6. The influence of compound **12b** on the inhibition of K^+ -pnppase activity from purified brain and kidney NAK preparations. Each point is the mean \pm SEM of 3 different experiments.

As emphasized by Li et al. [45], NAK was originally discovered as an ion pump that is essential for cell viability and provides a means for the epithelium to secrete and/or absorb solutes and nutrients. However, as elegantly demonstrated by Xie and Askari [46] and Liang et al. [47], in addition to pumping ions across the cell membrane, the α_1 subunit of NAK also functions as a scaffold and signal transduction molecule. In glioma cells, inhibiting NAK activity does not modify $[Ca^{2+}]_i$ and $[Na^+]_i$ but does massively induce non-apoptotic cell death [15]. Recently, a α_1 NAK/Src receptor complex has been identified as one of the central components of α_1 NAK-mediated signal transduction [48]. Furthermore, the Xie group [45] demonstrated the *in vivo* effectiveness in human tumor xenografts targeting NAK/Src-mediated signal transduction to develop new anticancer therapeutics.

Another signaling pathway controlled by NAK is the Ras/Raf/MEK/ERK1/2 pathway [49]. For example, translationally controlled tumor protein (TCTP) is implicated in cell growth and malignant transformation, and TCTP interacts directly with the third cytoplasmic domain of the α NAK subunits [50]. Jung et al. [50] have demonstrated that TCTP induces Src release from the α NAK subunit, Src activation and activation of the Ras/Raf/MEK/ERK1/2 pathway. However, Ras also controls NAK activity. For example, over a short time scale, fibroblast growth factor-10 (FGF-10) up-regulates NAK activity in alveolar epithelial cells (AECs) via the Grb-SOS/Ras/MAPK pathway [51]. AECs that express dominant negative Ras protein prevent FGF-10-mediated NAK recruitment to the AEC plasma membrane [51].

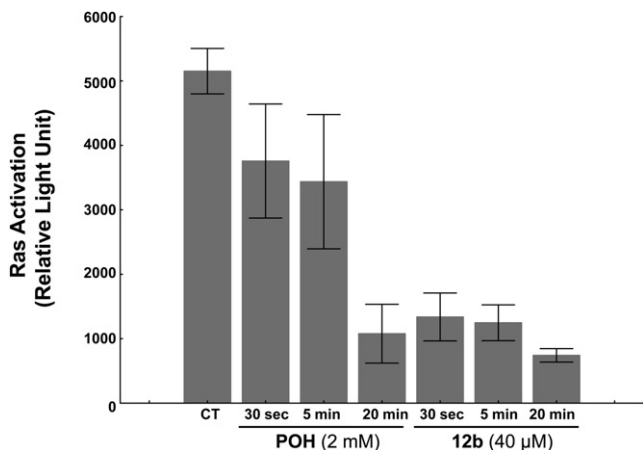


Fig. 7. Characterization of the Ras oncogene inhibitory profiles of POH (positive control) and compound **12b** in human Hs683 glioma cells. Each experimental condition was performed in triplicate. Data are presented as the mean \pm SEM.

Activity differences between purified and whole homogenate NAK can be used to indicate selectivity because nonspecific binding in crude homogenates decreases the compound's inhibitory effect on NAK [19]. Based on this criterion, the data shown in Fig. 4 indicate that **12b** was somewhat less selective toward the brain enzyme (mainly α_2 and α_3 isoforms) than the kidney enzyme (α_1 isoform), which showed the same IC_{50} values for purified and homogenate NAK activities. Other Mg^{++} -dependent ATPases in crude tissue homogenates were not affected by this compound at the concentrations used (0.1–1.0 mM). NAK inhibition by **12b** was thus uncompetitive with the substrate ATP. In this type of inhibition, the inhibitor does not bind to the enzyme alone. Rather, the inhibitor binds to the enzyme–substrate complex, which is, in this case, the ATP–NAK complex. Considering the two phases of the NAK catalytic cycle (I and II), these data indicate that compound **12b** acts on phase I of the NAK cycle. ATP first binds to the enzyme and then is the substrate for phosphorylation of the Na^+ activated-enzyme. POH displayed a similar behavior [19], but the inhibitory capacity of **12b** for the kidney isoform is approximately 3 times higher than the activity measured for POH. Interestingly, K^+ -pnppase activity, which measures phase II of the NAK cycle, was not affected by **12b** in purified kidney preparations, whereas some degree of inhibition was noted for the purified brain enzyme. The brain enzyme was also less selective to this compound described above. Therefore, at least for the kidney enzyme, **12b** seems to act primarily in phase I of the NAK cycle.

Despite these findings, it is still possible that compound **12b** directly binds to some NAK sites, and the possibility that it interacts with the lipid microenvironment surrounding the enzyme cannot be discharged. Notably, the lipid composition of brain and kidney cells is different.

In conclusion, the current study reveals that 4-bromo-2-(piperidin-1-yl)thiazol-5-yl-phenyl methanone (**12b**) displays *in vitro* growth inhibitory activity that partially relates to the inhibition of the α subunits of the Na^+/K^+ -ATPase. Furthermore, we observed some specificity of the compound toward the α_1 subunit, which is overexpressed in gliomas, melanomas and NSCLCs. The most potent anti-NAK inhibitors are cardiotonic steroids, which exhibit cardiotoxicity and have very narrow therapeutic indices as potential anticancer drugs. It is possible that **12b** will not display cardiotoxic effects as pronounced as the cardiotonic steroids; we are currently performing cardiotoxicity tests. Another non-cardiotonic steroid-related compound, POH, has already been demonstrated to contribute significant therapeutic benefits to glioma patients. POH exerts its anti-glioma effects at least partly through both α_1 NAK subunit and Ras oncogene inhibition. Notably, **12b** appears to be approximately 3 times more potent than POH in inhibiting α_1 NAK subunit activity and 40 times more potent than POH in inhibiting Ras activity.

5. Experimental section

5.1. Chemistry

5.1.1. General methods

All solvents were of reagent grade and were purified and dried by standard methods when necessary. All chemicals were purchased from Acros or Sigma–Aldrich. All reactions were routinely checked by TLC analysis on an Alugram SIL G/UV₂₅₄ (Macherey-Nagel) with spots visualized by UV light. The concentration of solutions after reactions and extractions involved the use of a rotary evaporator operating at reduced pressure. Organic solutions were dried over anhydrous magnesium sulfate, and column chromatography was performed using silica gel 60 (50–200 μ m diameter). Melting points were determined in open capillaries on a Stuart

SMP3 apparatus and are uncorrected. The ^1H and ^{13}C NMR spectra were measured on an AC Bruker 250 MHz spectrometer in DMSO- d_6 ; chemical shifts are reported in parts per million (ppm). All coupling constants (J) are given in Hz. MS spectra were recorded on an Agilent Technologies GC–MS instrument equipped with a 7683 injector, 6890 N gas chromatograph and a 5973 mass selective detector. The mass spectrometer was operated in EI mode at 70 eV, and MS spectra were recorded from m/z 50 to 650. Elemental analyzes (C, H, N, S) were used to confirm the purity of all compounds (>95%) and were performed on a CHN ThermoScientific Flash 2000 apparatus.

5.1.1.1. Synthesis of 2,5-substitued-4-halogeno-1,3-thiazole by Doyle's method. Twelve millimoles of either anhydrous copper (II) chloride or anhydrous copper (II) bromide were added to a solution of *tert*-butyl nitrite (15 mmol) in acetonitrile anhydrous (40 mL). The mixture was stirred at 50 °C for 1 h, and then 2,5-substitued 4-amino-1,3-thiazole was added slowly. The resulting mixture was stirred at room temperature overnight. The reaction mixture was quenched in water (100 mL). When the precipitate appeared, it was filtered, washed twice with 20 mL of water, and dried under room temperature until a constant weight was reached. The isolated solid was purified by recrystallization in isopropanol. When a viscous mixture appeared, the solution was extracted with ethyl acetate (3 × 25 mL). The organic layers were dried with MgSO_4 , filtered, and evaporated. The oily solid was then purified by column chromatography on silica gel.

We detail here below the characteristics of **12a** and **12b**. All remaining compounds under study are described in the [Supplemental Information](#) section.

5.1.1.2. (4-Chloro-2-(piperidin-1-yl)-1,3-thiazol-5-yl)(phenyl)methanone (12a). Yield, 59%; yellow solid; mp 145 °C; ^1H NMR (250 MHz, DMSO- d_6): δ 1.55 (m, 6H, 3 × CH_2), 3.55 (m, 4H, 2 × CH_2), 7.54 (m, 2H), 7.61 (m, 1H), 7.67 (m, 2H); ^{13}C NMR (62.5 MHz, DMSO- d_6): δ 23.0, 24.6, 48.6, 116.9, 128.0, 128.3, 131.7, 138.8, 142.1, 169.4, 185.4; HRMS calcd for $\text{C}_{15}\text{H}_{16}\text{ClN}_2\text{OS}$ [$\text{M} + \text{H}$] $^+$ 307.0666, found 307.0650. Anal. Calcd for $\text{C}_{15}\text{H}_{15}\text{ClN}_2\text{OS}$: C, 58.72; H, 4.93; N, 9.13; S, 10.45. Found: C, 58.32; H, 5.22; N, 9.32; S, 10.14.

5.1.1.3. (4-Bromo-2-(piperidin-1-yl)-1,3-thiazol-5-yl)(phenyl)methanone (12b). Yield, 93%; yellow solid; mp 123 °C; ^1H NMR (250 MHz, DMSO- d_6): δ 1.60 (m, 6H, 3 × CH_2), 3.52 (m, 4H, 2 × CH_2), 7.51 (m, 2H), 7.58 (m, 1H), 7.63 (m, 2H); ^{13}C NMR (62.5 MHz, DMSO- d_6): δ 23.1, 24.6, 48.7, 118.5, 128.1, 128.3, 131.2, 131.8, 138.8, 170.5, 185.7; HRMS calcd for $\text{C}_{15}\text{H}_{16}\text{BrN}_2\text{OS}$ [$\text{M} + \text{H}$] $^+$ 351.0161, found 351.0170. Anal. Calcd for $\text{C}_{15}\text{H}_{15}\text{BrN}_2\text{OS}$: C, 51.29; H, 4.30; N, 7.98; S, 9.13. Found: C, 51.18; H, 4.40; N, 7.98; S, 9.30.

5.1.1.4. Synthesis of methyl 6-substitued-2-(methylsulfanyl)thieno[2,3-d]thiazole-5-carboxylate. Methylthioglycolate (5 mmol) was dissolved in methanol (30 mL). Sodium methylate (5 mmol) was added, and the solution was stirred for 15 min at 60 °C. 5-substitued 4-halogeno-2-methylsulfanyl-1,3-thiazole was added, and the mixture was refluxed for 5 h. Then, fresh sodium methylate (6 mmol) was added and heated at 50° for 1 h. The mixture was poured into water (100 mL) with stirring. The precipitate was filtered, washed with water, and dried at room temperature overnight. The isolated solid was purified by recrystallization in isopropanol.

All compounds under study are described in the [Supplemental Information](#) section.

5.1.1.5. Synthesis of methyl 6-methyl-2-(substitued)thieno[2,3-d][1,3]thiazole-5-carboxylate 14. (3 mmol) and the corresponding amine (10 mL) were refluxed overnight. The mixture was poured

into water (80 mL) while stirring. The precipitate was filtered, washed with water, and dried at room temperature overnight. The isolated solid was purified by recrystallization in isopropanol.

All compounds under study are described in the [Supplemental Information](#) section.

5.2. Stability test

5.2.1. Solvents

Formic acid (FA) and high-purity LC-MS methanol (MeOH) were purchased from Merck (Darmstadt, Germany). Water was purified using a Milli-Q purification system from Millipore (Bedford, MA, USA).

5.2.2. Infusion-MS analysis

Compounds **12a** and **12b** were dissolved in DMSO (5 mM). Before injection, these solutions were diluted 100-fold in water or in RPMI. Analyzes were performed using a Rapid Resolution Liquid Chromatography (RRLC) 1200 series from Agilent Technologies (Santa Clara, CA, USA) coupled to a 6520 series electrospray ion source (ESI) – quadrupole time-of-flight (QTOF) from Agilent Technologies. One microliter of samples was infused using a bypass and FA 0.2%–MeOH 50–50 (v/v) as solvent. The stability test has been performed at 37 °C for 72 h for each compound. The ESI-QTOF parameters were: positive mode, extended dynamic range mode (2 GHz), gas temperature of 300 °C, drying gas of 9 l/min, nebulizer pressure of 40 psi, capillary voltage of 3000 V, fragmentor 90 V and MS scan range of 110–950 m/z at 6 spectra/s. Data were acquired by the Mass Hunter Acquisition® software from Agilent Technologies and analyzed by the Mass Hunter Qualitative Analysis® software (AgilentTechnologies). Compounds were identified by their molecular peak and their adducts merged into one chromatogram for each compound: 307.0666 m/z [$\text{M} + \text{H}$] $^+$, 329.0486 m/z [$\text{M} + \text{Na}$] $^+$ and 345.0225 m/z [$\text{M} + \text{K}$] $^+$ for compound **12a** and 351.0161 m/z [$\text{M} + \text{H}$] $^+$, 372.9981 m/z [$\text{M} + \text{Na}$] $^+$ and 388.9720 m/z [$\text{M} + \text{K}$] $^+$ for compound **12b**.

5.3. Pharmacology

5.3.1. Determination of in vitro anticancer activity

The histological types and origins of the six cancer cell lines that were used for the MTT colorimetric assay are detailed in the legend of [Table 2](#). The cells were cultured in RPMI (Lonza, Verviers, Belgium) medium supplemented with 10% heat inactivated fetal calf serum (Lonza). All culture media were supplemented with 4 mM glutamine, 100 $\mu\text{g}/\text{mL}$ gentamicin, 200 U/mL penicillin and 200 $\mu\text{g}/\text{mL}$ streptomycin (Lonza).

Normal astrocytes were obtained as detailed previously [40]. Briefly, neonatal NMRI mouse cortices were freed of meninges, minced into small pieces of tissue with microscissors and then suspended in MEM (Invitrogen) supplemented with glucose 6 g/L and 10% fetal calf serum (FCS; Invitrogen). The cell suspension was then filtered through a 225 μm -pore and a 25 μm -pore filter. The filtered cell suspension was plated on an uncoated T25 flask for 72 h. The medium was then changed, and the cells were grown until confluence.

The overall growth level of the human cancer cell lines was determined using a colorimetric MTT (3-[4,5-dimethylthiazol-2-yl]-diphenyl tetrazolium bromide, Sigma, Belgium) assay as detailed previously [15–17]. Each experimental condition was performed in six replicates.

5.3.2. Computer-assisted phase contrast microscopy (quantitative videomicroscopy)

The direct visualization of compound-induced effects, in terms of cytotoxicity versus cytostaticity, in human Hs683 glioma cells was performed as detailed elsewhere [15,17,23].

5.3.3. Biochemical characterization of anti- Na^+/K^+ -ATPase activity

Guinea pig brains and kidneys were used in the preparation of homogenates and Na^+/K^+ -ATPase-enriched fractions. Guinea pigs were kept in compliance with the Guide for the Care and Use of Laboratory Animals (US Department of Health and Human Services, N.I.H.) and in accordance with regulations of our institution.

Lyophilized Na^+/K^+ -ATPase enriched fractions were prepared according to a modification of the Jørgensen protocol [52] as detailed previously [53]. The specific activities of the purified enzymes were 106 $\mu\text{mol Pi/h/mg}$ of protein (brain) and 100 $\mu\text{mol Pi/h/mg}$ of protein (kidney). Protein assays were performed by Peterson's method [54].

Na^+/K^+ -ATPase activity was determined in microtiter plates as described previously [53]. The final reaction volume (120 μL) contained 110 mM NaCl, 20 mM KCl, 5 mM MgCl_2 , 50 mM Tris–HCl pH 7.6, inhibitor solutions (absent in controls), an enzyme preparation and 5 mM ATP. The amount of the enzyme preparation used in all experiments (including tissue homogenates) corresponded to an activity of 0.12–0.13 $\mu\text{mol Pi formed/h}$ in the control assays (100% enzyme activity). In the blanks, the enzyme was added only after the reaction had been stopped. Compound **12b** was dissolved in dimethyl sulfoxide (DMSO) and diluted with an adequate volume of distilled water to keep the DMSO concentration in the incubation mixture below 2% (V/V), a condition that did not affect the enzyme activity. Preparations were pre-incubated at 37 °C for 10 min before starting the enzyme reaction with ATP, and the reaction was stopped 30 min later. The Na^+/K^+ -ATPase activity of crude homogenates was calculated as the difference between total ATPase activity in absence of ouabain and ouabain-insensitive ATPase activity (Mg^{++} -ATPases); 3.6 mM ouabain was used for these measurements. For the kinetic studies with varying Na^+ , K^+ or ATP concentrations, the inhibitor compound was kept at a fixed concentration corresponding to its IC_{50} .

K^+ -activated-*p*-nitrophenyl phosphatase activity was analyzed according to the procedure detailed by Rodriguez de Lores Arnaiz [55]. For basal measurements, KCl was omitted and substituted with 1 mM ouabain. K^+ -pnppase activity was calculated as the difference between the total and basal activity measurements.

5.3.4. Biochemical characterization of anti-Ras oncogene activity

The Hs683 glioma cells were treated with 40 μM **12b** for 30 s or with 2 mM POH for 5 and 20 min. The activation of Ras was measured using an ELISA-based kit from Active Motif (Ras GTPase Chemi ELISA Kit, ref. 52097, Active Motif, Rixensart, Belgium). The kit was used according to the manufacturer's instructions. Briefly, after the treatment, Hs683 glioma cells were washed in PBS, scraped in Complete/Lysis Binding Buffer, and incubated for 15 min on ice. Next, the cells were centrifuged for 10 min at 14,000 rpm at 4 °C. The supernatant was collected, and the protein content was measured. In this assay, 100 μg of protein was used. The first step of the Ras GTPase Chemi ELISA is the binding of Ras. The GST-Raf-RBD that contains a Ras-Binding Domain is used to capture activated Ras onto the glutathione-coated plate. This GST-Raf-RBD is diluted in Complete/Lysis Binding Buffer, added to each well of the plate and incubated for 1 h at 4 °C with mild agitation (100 rpm). The plate is then washed 3 times with the wash buffer. The samples (**12b**-versus POH-treated Hs683 cells) and the negative control (untreated Hs683 glioma) were loaded on the plate and incubated for 1 h at room temperature with mild agitation (100 rpm). Each well was washed 3 times with wash buffer and incubated for 1 h at room temperature with the diluted primary antibody (H-Ras antibody) and then washed an additional three times. The secondary antibody (HRP conjugated antibody) was added for 1 h at room temperature, and the plate was washed four times after this incubation. The Chemiluminescent Working Solution was added to each well, and

the chemiluminescence was read within 15 min after the addition of the Chemiluminescent working solution using a luminometer (ActiveGlo LR-100 luminometer, DSLabs, USA).

Acknowledgments

R.K. is a Director of Research with the Fonds National de la Recherche Scientifique (FNRS, Belgium). G.K. thanks Alzchem GmbH (Trostberg, Germany) for a gift of cyanamide. We also warmly thank Thierry Gras for his excellent technical assistance.

Appendix A. Supplementary data

Supplementary data related to this article can be found at <http://dx.doi.org/10.1016/j.ejmech.2013.01.046>.

References

- [1] T. Cloughesy, The impact of recent data on the optimization of standards of care in newly diagnosed glioblastoma, *Semin. Oncol.* 38 (2011) S11–S20.
- [2] S.J. Schramm, A.E. Campain, R.A. Scolyer, Y.H. Yang, G.J. Mann, Review and cross-validation of gene expression signatures and melanoma prognosis, *J. Invest. Dermatol.* 132 (2011) 274–283.
- [3] L.L. Carr, J.H. Finigan, J.A. Kern, Evaluation and treatment of patients with non-small cell lung cancer, *Med. Clin. North. Am.* 95 (2011) 1041–1054.
- [4] F. Lefranc, J. Brotchi, R. Kiss, Possible future issues in the treatment of glioblastomas, with a special emphasis on cell migration and the resistance of migrating glioblastoma cells to apoptosis, *J. Clin. Oncol.* 23 (2005) 2411–2422.
- [5] M.S. Soengas, S.W. Lowe, Apoptosis and melanoma chemoresistance, *Oncogene* 22 (2003) 3138–3151.
- [6] S. Han, J. Roman, Targeting apoptotic signaling pathways in human lung cancer, *Curr. Cancer Drug Targets* 10 (2010) 566–574.
- [7] P. Savage, J. Stebbing, M. Bower, T. Crook, Why does cytotoxic chemotherapy cure only some cancers? *Nat. Clin. Pract. Oncol.* 6 (2009) 43–52.
- [8] T.R. Wilson, P.G. Johnston, D.B. Longley, Anti-apoptotic mechanisms of drug resistance in cancer, *Curr. Cancer Drug Targets* 9 (2009) 307–319.
- [9] C.E. Griguer, C.R. Oliva, Bioenergetics pathways and therapeutic resistance in gliomas: emerging role of mitochondria, *Curr. Pharm. Des.* 17 (2011) 2421–2427.
- [10] C.A. La Porta, Mechanism of drug sensitivity and resistance in melanoma, *Curr. Cancer Drug Targets* 9 (2009) 391–397.
- [11] G.V. Scagliotti, G. Novello, G. Selvaggi, Multidrug resistance in non-small-cell lung cancer, *Ann. Oncol.* 10 (1999) S83–S86.
- [12] R. Stupp, M.E. Hegi, W.P. Mason, M.J. van den Bent, M.J. Taphoorn, R.C. Janzer, S.K. Ludwin, A. Allgeier, B. Fisher, K. Belanger, et al., Effects of radiotherapy with concomitant and adjuvant temozolomide versus radiotherapy alone on survival in glioblastoma in a randomised phase III study: 5-years analysis of the EORTC-NCIC trial, *Lancet Oncol.* 10 (2009) 459–466.
- [13] F. Lefranc, V. Facchini, R. Kiss, Pro-autophagic drugs: a novel means to combat apoptosis-resistant cancers, with a special emphasis on glioblastomas, *Oncologist* 12 (2007) 1395–1403.
- [14] T. Mijatovic, F. Dufresne, R. Kiss, Cardiotonic steroids-mediated targeting of the Na^+/K^+ -ATPase to combat chemoresistant cancers, *Curr. Med. Chem.* 19 (2012) 627–646.
- [15] F. Lefranc, T. Mijatovic, Y. Kondo, S. Sauvage, I. Roland, O. Debeir, D. Krstic, V. Vasic, P. Gailly, S. Kondo, G. Blanco, R. Kiss, Targeting the alpha-1 subunit of the sodium pump to combat glioblastoma cells, *Neurosurgery* 62 (2008) 211–221.
- [16] V. Mathieu, C. Pirker, E. Martin de Lassalle, M. Vernier, T. Mijatovic, N. De Neve, J.F. Gaussin, M. Dehoux, F. Lefranc, W. Berger, R. Kiss, The sodium pump alpha-1 subunit: a disease progression-related target for metastatic melanoma treatment, *J. Cell. Mol. Med.* 13 (2009) 3960–3972.
- [17] T. Mijatovic, I. Roland, E. Van Quaquebeke, B. Nilsson, A. Mathieu, F. Van Vynckt, F. Darro, G. Blanco, V. Facchini, R. Kiss, The alpha-1 subunit of the sodium pump could represent a novel target to combat non-small cell lung cancers, *J. Pathol.* 121 (2007) 170–179.
- [18] T. Mijatovic, U. Jungwirth, P. Heffeter, M.A. Hoda, R. Dornetshulber, R. Kiss, W. Berger, The Na^+/K^+ -ATPase is the Achilles heel of multi-drug-resistant cancer cells, *Cancer Lett.* 282 (2009) 30–34.
- [19] D.G. Garcia, L.M.F. Amorim, M.V. de Castro Faria, A.S. Freire, R.E. Santelli, C.O. Da Fonseca, T. Quirico-Santos, P. Burth, The anticancer drug perillyl alcohol is a Na^+/K^+ -ATPase inhibitor, *Mol. Cell. Biochem.* 345 (2010) 29–34.
- [20] C.O. Da Fonseca, J.T. Silva, I.R. Lins, M. Simao, A. Arnobio, D. Futuro, T. Quirico-Santos, Correlation of tumor topography and peritumoral edema of recurrent malignant gliomas with therapeutic response to intranasal administration of perillyl alcohol, *Invest. New Drugs* 27 (2009) 557–564.
- [21] C.O. Da Fonseca, M. Simao, I.R. Lins, R.O. Caetano, D. Futuro, T. Quirico-Santos, Efficacy of monoterpene perillyl alcohol upon survival rate of patients with recurrent glioblastoma, *J. Cancer Res. Clin. Oncol.* 137 (2011) 287–293.

- [22] P. Dumont, L. Ingrassia, S. Rouzeau, F. Ribaucour, S. Thomas, I. Roland, F. Darro, F. Lefranc, R. Kiss, The Amaryllidaceae isocarboxystiril narciclasine induces apoptosis by activation of the death receptor and/or mitochondrial pathways in cancer cells but not in normal fibroblasts, *Neoplasia* 9 (2007) 766–776.
- [23] L. Ingrassia, F. Lefranc, J. Dewelle, L. Pottier, V. Mathieu, S. Spiegl-Kreinecker, S. Sauvage, M. El Yazidi, M. Dehoux, W. Berger, E. Van Quaquebeke, R. Kiss, Structure-activity relationship analysis of novel derivatives of narciclasine (an Amaryllidaceae isocarboxystiril derivative) as potential anticancer agents, *J. Med. Chem.* 52 (2009) 1100–1114.
- [24] G. van Goietsenoven, J. Hutton, J.P. Becker, B. Lallemand, F. Robert, F. Lefranc, C. Pirker, G. Vandenbussche, P. Van Antwerpen, A. Evidente, W. Berger, M. Prévost, J. Pelletier, R. Kiss, T.G. Kinzy, A. Kornienko, V. Mathieu, Targeting of eEF1A with Amaryllidaceae isocarboxystirils as a strategy to combat melanomas, *FASEB J.* 24 (2010) 4575–4584.
- [25] A. Mathieu, M. Remmelink, N. D'Haene, S. Penant, J.F. Gaussin, R. Van Ginckel, F. Darro, R. Kiss, I. Salmon, Development of a chemoresistant orthotopic human non-small cell lung carcinoma model in nude mice, *Cancer* 101 (2004) 1908–1918.
- [26] S.A. Holstein, R.J. Hohl, Monoterpene regulation of Ras and Ras-related protein expression, *J. Lipid Res.* 44 (2003) 1209–1215.
- [27] C.O. Da Fonseca, R. Linden, D. Futuro, C.R. Gattass, T. Quirico-Santos, Ras pathway activation in gliomas: a strategic target for intranasal administration of perillyl alcohol, *Arch. Immunol. Ther. Exp.* 56 (2008) 267–276.
- [28] A.T. Parsa, E.C. Holland, Cooperative translational control of gene expression by Ras and Akt in cancer, *Trends Mol. Med.* 10 (2004) 607–613.
- [29] H.W. Lo, Targeting Ras-Raf-ERK and its interactive pathways as a novel therapy for malignant gliomas, *Curr. Cancer Drug Targets* 10 (2010) 840–848.
- [30] D. Thomae, E. Perspicace, Z. Xu, D. Henryon, S. Schneider, S. Hesse, G. Kirsch, P. Seck, One-pot synthesis of new 2,4,5-trisubstituted 1,3-thiazoles and 1,3-selenazoles, *Tetrahedron* 65 (2009) 2982–2988.
- [31] D. Thomae, E. Perspicace, S. Hesse, G. Kirsch, P. Seck, Synthesis of substituted [1,3]thiazolo[4,5-b]pyridines and [1,3]thiazolo[4,5-d][1,2,3]triazines, *Tetrahedron* 64 (2008) 9309–9314.
- [32] M.P. Doyle, B. Siegfried, J.F. Dellaria, Alkyl nitrite-metal halide deamination reactions. 2. Substitutive deamination of arylamines by alkyl nitrites and copper (II) halides. A direct and remarkably efficient conversion of arylamines to aryl halides, *J. Org. Chem.* 42 (1977) 2426–2431.
- [33] A. Begouin, S. Hesse, M.J.R.P. Queiroz, G. Kirsch, Synthesis of diarylamines in the thiophenes series by Buchwald–Hartwig coupling, *Synthesis* 14 (2005) 2373–2378.
- [34] K.J. Hodgetts, M.T. Kershaw, Regiocontrolled synthesis of substituted thiazoles, *Org. Lett.* 4 (2002) 1363–1365.
- [35] P. Stanetty, T. Dvorak, M.D. Mihovilovic, Synthesis of thieno[2,3-d]thiazole-6-carboxylic acid derivatives as potential inducers of systemic resistance in plants, *Arkivoc*, part ii, 2001, pp. 34–41.
- [36] I.V. Zavarzin, N.G. Smirnova, V.N. Yarovenko, M.M. Krayushkin, Synthesis of thieno[2,3-d]thiazole-2-carboxamides, *Russ. J. Org. Chem.* 40 (2004) 137–139.
- [37] S.P.G. Costa, A.M.F. Oliveira-Campos, G. Kirsch, J. Griffiths, Synthesis of thieno [2,3-d]thiazole derived dyes with potential application in nonlinear optics, *An. Quim. Int. Ed.* 94 (1998) 186–188.
- [38] S. Athmani, B. Iddon, Azoles. Synthesis of derivatives of thieno[2,3-d]thiazole, 4H-pyrrolo[2,3-d]thiazole, 2H-pyrazolo[3,4-d]thiazole and isoxazolo[3,4-d]thiazole from thiazolidine-2,4-dione, *J. Chem. Soc. Perkin Trans. 1* 8 (1992) 973–977.
- [39] S. Athmani, B. Iddon, Azoles. Part 10. Thiazolo[4',5':4,5]thieno[3,2-d]pyrimidine, a new heterocyclic ring system, *Tetrahedron* 48 (1992) 7689–7702.
- [40] E. Goffin, D. Lamoral-Theys, N. Tadjidine, P. de Tullio, L. Mondin, F. Lefranc, P. Gailly, B. Rogister, R. Kiss, B. Pirotte, Benzopyrans display *in vitro* anticancer activity and selectivity on apoptosis-resistant glioblastoma cells: screening, synthesis of simplified derivatives, and structure-activity relationship analysis, *Eur. J. Med. Chem.* 54 (2012) 834–844.
- [41] R. Kiss, Hot topics in ion channels and cancers, *Curr. Med. Chem.* 19 (2012) 625–626.
- [42] I. Prassas, E.P. Diamandis, Novel therapeutic applications of cardiac glycosides, *Nat. Rev. Drug Discov.* 7 (2008) 926–935.
- [43] E.A. Platz, S. Yegnasubramanian, J.O. Liu, C.R. Chong, J.S. Shim, S.A. Kenfield, M.J. Stampfer, W.C. Willet, B. Giovannucci, W.G. Nelson, A novel two-stage, transdisciplinary study identifies digoxin as a possible drug for prostate cancer treatment, *Cancer Discovery* 1 (2011) 68–77.
- [44] J.T. Belanger, Perillyl alcohol: applications in oncology, *Altern. Med. Rev.* 3 (1998) 448–457.
- [45] Z. Li, Z. Zhang, J.X. Xie, X. Li, J. Tian, T. Cai, H. Cui, H. Ding, J.I. Shapiro, Z. Xie, Na/K-ATPase mimetic pNaKtide peptide inhibits the growth of human cancer cells, *J. Biol. Chem.* 286 (2011) 32393–32403.
- [46] Z. Xie, A. Askari, Na⁺/K⁺-ATPase as a signal transducer, *Eur. J. Biochem.* 269 (2002) 2434–2439.
- [47] M. Liang, J. Tian, L. Liu, S. Pierre, J. Liu, J. Shapiro, Z.J. Xie, Identification of a pool of non-pumping Na/K-ATPase, *J. Biol. Chem.* 282 (2007) 10585–10593.
- [48] J. Tian, T. Cai, Z. Yuan, H. Wang, L. Liu, M. Haas, E. Maksimova, X.Y. Huang, Z.J. Xie, Binding of Src to Na⁺/K⁺-ATPase forms a functional signaling complex, *Mol. Biol. Cell.* 17 (2006) 317–326.
- [49] L. Zhang, Z. Zhang, H. Guo, Y. Wang, Na⁺/K⁺-ATPase-mediated signal transduction and Na⁺/K⁺-ATPase regulation, *Fundam. Clin. Pharmacol.* 22 (2008) 615–621.
- [50] J. Jung, H.Y. Kim, M. Kim, K. Sohn, M. Kim, K. Lee, Translationally controlled tumor protein induces human breast epithelial cell transformation through the activation of Src, *Oncogene* 30 (2011) 2264–2274.
- [51] D. Upadhyay, E. Lecuona, A. Comellas, D.W. Kamp, J.L. Sznajder, Fibroblast growth factor-10 upregulates Na, K-ATPase via the MAPK pathway, *FEBS Lett.* 545 (2003) 173–176.
- [52] P.L. Jørgensen, Purification and characterization of (Na⁺, K⁺)-ATPase. III. Purification from the outer medulla of mammalian kidney after selective removal of membrane components by sodium dodecylsulphate, *Biochim. Biophys. Acta* 356 (1977) 36–52.
- [53] P. Burth, M. Younes-Ibrahim, F.H.F.S. Gonçalves, E.R. Costa, M.V. Castro Faria, Purification and characterization of a Na⁺, K⁺ ATPase inhibitor found in an endotoxin of leptospira, *Infect. Immun.* 65 (1997) 2557–2560.
- [54] G.L. Peterson, A simplification of the protein assay method of Lowry et al. which is more generally applicable, *Anal. Biochem.* 83 (1977) 346–356.
- [55] G.G. Rodriguez de Lores Arnaiz, T. Herbin, C. Pena, A comparative study between a brain Na⁺, K⁺-ATPase inhibitor (endobain E) and ascorbic acid, *Neurochem. Res.* 28 (2003) 903–910.